CrossMark

Evaluation of the Pore Structure of Reservoirs Based on NMR T_2 Spectrum Decomposition

Fei-Fei Wang[1] · Tian-Zhi Tang[2] · Tang-Yan Liu[1] · Hai-Ning Zhang[2]

Abstract Nuclear magnetic resonance (NMR) T_2 distributions can be employed to understand the geometry of pores, but they are not sensitive enough to determine pore connectivity. In this paper, the pore space in reservoirs is regarded as a series of different sizes of the combination of spherical pores and cylinder pores based on the pore network model and Sphere–Cylinder model. In terms of the optimized T_2 inversion method, T_2 spectral distribution is decomposed into two groups, sphere pore distribution and cylinder pore distribution. It is assumed that cylinder pore controls the connectivity and permeability of the reservoir and the sphere pore is the main place of fluid storage. The more cylinder pores that exist, the better the connectivity and permeability are. The data of eight core plugs are analyzed using this method, and the results are in accordance with those of core analysis, which proves the practicability of our research and provides a basis for the direct evaluation of reservoir pore structure using NMR T_2 distribution.

1 Introduction

The pore structure of reservoir rocks is defined by the geometry, connectivity, size and distribution of pores, pore throats, and the pore–pore throat aspect ratio [1]. Because the pore structure controls the electrical property, oil and gas production as well as the seepage characteristics of the reservoir, it is of great significance to reveal the pore structure of a reservoir for the oil and gas exploration [2–6].

The pore size distribution is usually determined using mercury injection capillary pressure (MICP) by injecting mercury and measuring the volume as a function of

✉ Fei-Fei Wang
1105936347@qq.com

1 State Key Lab of Marine Geology, Tongji University, Shanghai 200092, China

2 Technology Research Center, China Petroleum Logging CO. LTD., Xi'an 710077, China

applied pore pressure [7–9]. However, this method is not applicable to in situ measurements. Borehole nuclear magnetic resonance (NMR) measurement has been among the most reliable techniques to evaluate porosity and pore size distribution in porous media [10]. There have been many publications on the basic principles and applications of this technique in petrophysical studies in various formations [11]. since the mechanism of proton relaxation in restricted space and porous media was derived and studied decades ago [12]. NMR logging can present the information of the pore structure in a continuous, rapid and nondestructive way; correlation analysis between MICP and NMR T_2 distribution has been used to estimate the pore size distribution [13–15]. However, it is very difficult to obtain good results if only the correlation is used. This is partly because MICP is relative to the pore space accessed by a certain pore throat size, but not to the distribution of the total pore size; however, NMR T_2 is related to the pore radius (pores and pore throats).

The widely used interpretation method for NMR relaxometry is the NMR T_2 distribution. There are three NMR relaxation mechanisms that influence T_2 relaxation times: grain surface relaxation, relaxation by molecular diffusion in magnetic field gradients and relaxation by bulk fluid process [16–19]. In the fast diffusion limit, the relaxation time T_2 of hydrogen nuclei in the fluids in porous media, can be expressed as:

$$\frac{1}{T_2} = \frac{1}{T_{2B}} + \frac{1}{T_{2S}} + \frac{1}{T_{2D}} = \frac{1}{T_{2B}} + \rho \left(\frac{S}{V}\right)_{pore} + \frac{D(\gamma G T_E)^2}{12} \tag{1}$$

where T_{2B} is the bulk relaxation time, T_{2S} is the surface relaxation time, and T_{2D} is the diffusion-induced relaxation time. In the expressions for T_{2S} and T_{2D} on the right hand side, ρ_2 is the surface relaxivity, S/V is the surface-to-volume radio of the pore space, D is the diffusion coefficient of pore fluids, γ is the gyromagnetic ratio of a proton, G is the internal magnetic field gradient, and T_E is the inter-echo spacing time.

Grain surface relaxation-Molecules in fluids are in constant motion-Brownian motion-and diffuse about a pore space, hitting the grain surface several times during one NMR measurements. Researchers have shown that in most rocks, grain-surface relaxation is the most important influence on T_2. However, rocks with a high content of iron or other magnetic minerals have larger than usual values of ρ_2, hence, shorter NMR relaxation times and T_2 peak value shifts towards shorter relaxation time. Pore size also plays an important role in surface relaxation. The speed of relaxation depends on how frequently protons can collide with the surface and this depends on the surface-to-volume ratio (S/V) [18, 19].

It has been all accepted that NMR T_2 distribution represents the pore size distribution of a rock sample when (a) the pore space is fully water-saturated, (b) short T_E in the Carr-Purcell-Meiboom-Gill (CPMG) pulse sequence is used, and (c) all the pore surface has a uniform surface relaxivity value of ρ_2. Under these conditions the relaxation process is dominated by the surface relaxation mechanism, and the surface relaxation time, T_2, can be considered as directly proportional to the pore size, given by [10]:

$$\frac{1}{T_2} = \rho_2 \left(\frac{S}{V}\right)_{pore} \propto \left(\frac{1}{d}\right)_{pore} \tag{2}$$

where d is the diameter of the pores. However, to validate the equation, another assumption must be made: all the pores are similar in geometry (i.e. they all have similar surface-to-volume ratios). The surface-to-volume ratios of spherical pores and cylinder pores are given by:

$$\left(\frac{S}{V}\right)_{sphere} = \left(\frac{6}{d}\right)_{sphere} \tag{3}$$

and

$$\left(\frac{S}{V}\right)_{cylinder} = \left(\frac{4}{d}\right)_{cylinder} \tag{4}$$

If we consider the NMR relaxation response of a single water-filled pore, the transverse magnetization signal is described by an exponential decay [20]:

$$M(t) = \varphi e^{-t/T_2} \tag{5}$$

where the initial signal amplitude φ is proportional to the number of hydrogen nuclei (directly related to the pore volume). In a rock or sediment with a distribution of pore types, it's conventionally assumed that each pore contributes to the NMR signal in isolation and the observed signal is modeled as multi-exponential decay:

$$M(t) = \sum_i^n \varphi_i e^{-t/T_{2i}} \tag{6}$$

where the amplitude of φ_i is proportional to the volume of water-filled porosity associated with a corresponding relaxation time T_{2i}. Using this model of isolated pores, the $M(t)$ data are inverted to obtain a T_2 distribution by conjugate gradient (CG) method (Appendix 1), which is scaled according to Eq. (2) to estimate a pore-size distribution assuming uniform surface relaxivity and a simple pore shape (spherical pores or cylinder pores).

In this paper, we focus on the need for the evaluation of structure of reservoirs by using NMR logging data in field work. Consequently, some theoretical analysis must be done first to support the foundation of this method which will be discussed in following sections.
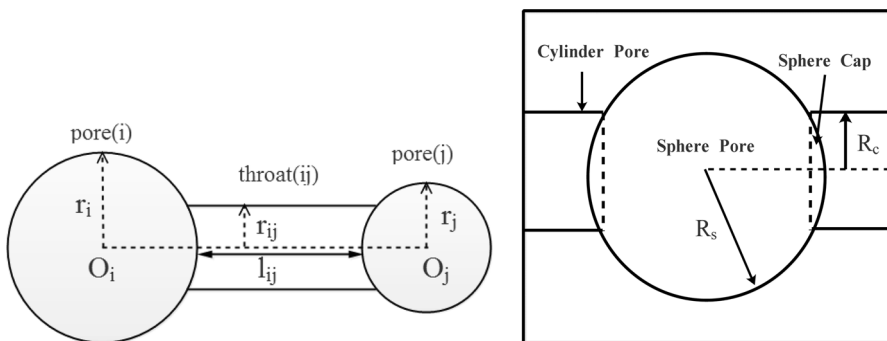
2 Pore Structure Model

Different types of pores may contact each other in various forms in reservoir rocks with complex interconnected relationships, especially as the pore configurations change greatly. Thus, it is difficult to totally simulate the real pore structure. Research is always focused on how to develop a model to approximate the real porous medium.

The capillary bundle model regards the pore network of porous medium as a bunch of capillary tubes with equivalent lengths and cross-sectional areas, as is shown in Fig. 1. Each single capillary tube follows the law and *Darcy* law. This model is easily solvable as well as accessible to geologists. However, the capillary bundle model is too simple because (a) there is no across connectivity between capillary tubes and (b) every capillary tube is straight without change in diameter [1].

To describe the pore structure in more detail, Fatt [21] proposed the concept of a pore network model for the first time by simulating the formation pores into a pore network composed of pores and throats (e.g. Fig. 2, on the left side). Pore controls the storage of fluid and throat controls the transfusion of fluid. Kewen et al. [22] built a three-dimensional irregular network model to study the characteristics of T_2 distribution in water-saturated rocks. The study focuses on the numerical simulations of correlation between T_2 distribution and pore-throat size distribution, throat radius, pore-throat ratio and connectivity. Liu et al. proposes the Sphere–Cylinder model (Fig. 3, on the right side) by assuming that pores in rock could be equivalent to a pore system composed of spherical pores and cylinder pores. Pores are divided into groups according to pore size, and the relaxation time of each group can be calculated with the Sphere–Cylinder model. With the relaxation time being the bin set of T_2 spectrum inversion, the echo signal of core samples could be inversed into T_2 distribution [23–25].
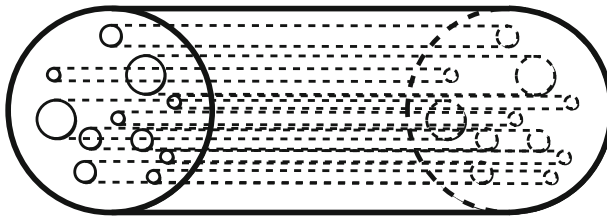
Fig. 1 Capillary bundle model

Fig. 2 Pore and throat in pore network model (*left*) and Sphere–Cylinder model (*right*)
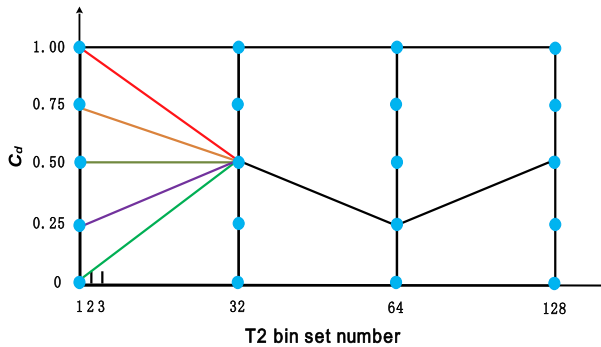
Fig. 3 Pathway scanning of Sphere–Cylinder model

3 T_2 Spectrum Decomposition Method

Ge et al. [26] proposed an automatic pore structure classification and discrimination method based on the T_2 spectrum decomposition for the carbonate reservoir of which the classification of reservoir pore structure is extremely difficult because of the multi-type pore space, strong heterogeneity and complex pore structure. The method is useful for core analysis, but NMR well logging data is not processed in his paper.

According to the Sphere–Cylinder model, pores in rock are divided into groups by pore size, and the number of groups is the same with that of bin set of relaxation signal inversion. Assume that one certain group of pores has the maximum equivalent sphere radius Re, which corresponds to the minimum cubic of side length $2Re$. In the pure spherical pores, the relationship between relaxation time and pore radius is given by Eqs. (2) and (3), which can be rewritten as:

$$R_e = 3\rho_2 T_2 \tag{7}$$

The overlapping part between the sphere and cylinder is the sphere cap, of which the height is h. The superficial area and volume of the sphere and cylinder in a Sphere–Cylinder model can be derived from the following equation:

$$\begin{cases} h = R_s - \sqrt{R_s^2 - R_c^2} \\ S_s = 4\pi R_s^2 - 4\pi R_s h \\ V_s = \frac{4}{3}\pi R_s^3 - \frac{2}{6}\pi h\left(3R_c^2 + h^2\right) \\ V_c = 2\pi R_c^2\left(R_e - \sqrt{R_s^2 - R_c^2}\right) \\ S_c = 4\pi R_c\left(R_e - \sqrt{R_s^2 - R_c^2}\right) + 2\pi R_c^2 \end{cases} \tag{8}$$

This equation could not be solved without a constraint condition. On the other hand, pores are not coupled; namely, each Sphere–Cylinder model is constrained into a corresponding cubic. Here gives the superficial area constraint condition:

$$\begin{cases} S_e = S_c + S_s \Rightarrow 4\pi R_e^2 = S_c + S_s \\ C_d = \dfrac{R_c}{R_s} \end{cases} \tag{9}$$

By substituting Eq. (9) into Eq. (8), we then obtain the solution and the optimal T_2 bin set for the inversion of relaxation signal.

$$\begin{cases} R_s = \dfrac{-b + \sqrt{b^2 + 4aR_e^2}}{2a} \\ b = C_d R_e \\ a = \dfrac{1}{2} C_d^2 - C_d \sqrt{1 - C_d^2} + \sqrt{1 - C_d^2} \end{cases} \tag{10}$$

$$\Rightarrow T_2(C_{di}) = \left(\frac{V_s + V_c}{(S_s + S_c)\rho_2} \right)_i$$

If we regard the point of T_2 spectrum as the contribution of the pores in a certain range of size, then the whole T_2 spectrum is the contribution of all the pores in core plug. The certain pores in rock are equivalent to corresponding Sphere–Cylinder model, hence, the pores can be divided into spherical pores and cylinder pores by superficial area coefficient or the volume coefficient. The volume coefficient is expressed as:

$$\begin{cases} A_{ci} = A_i \dfrac{V_{ci}}{V_{si} + V_{ci}} \\ A_{si} = A_i \dfrac{V_{si}}{V_{si} + V_{ci}} \end{cases} \tag{11}$$

where A_i, A_{ci} and A_{si} are the amplitude of total T_2 spectrum, cylinder T_2 spectrum and spherical T_2 spectrum among the i-th point, respectively. V_{ci} and V_{si} are the volume of cylinder pores and spherical pores among the i-th point, respectively.

The Sphere–Cylinder model uses the pre-selected radius ratio between cylinder and sphere C_d to calculate a new group of T_2 bin set for the inversion of T_2 distribution. Here, we propose the concept of 'pathway' to describe the C_d of each bin set (Fig. 3). Every pathway corresponds to a T_2 spectrum, among which we choose the optimal T_2 spectrum, namely, when a T_2 distribution fits the relaxation signal in the least squares, the pore structure defined by the Sphere–Cylinder model characterizes the pore system in rock best.

Different pathway will result in different characteristics of pore structure, hence, different T_2 decomposition results. Take three core plugs for example (Fig. 4), NMR T_2 measurements were performed on fully water saturated plugs with the salinity of 44,571.75 ppm under the temperature of 25 degrees centigrade. The T_2 distributions were generated with a T_E of 0.2 ms and 128 log-spaced inversion recovery steps ranging from 0.1 to 20,000 ms as well as the echo number is 8192.

From Fig. 4, on the first pathway (on the top), spherical pores are dominated within small pores and cylinder pores are developed within big pores, corresponds to favorable seepage characteristics; on the second pathway (on the middle), cylinder pores are developed among the whole pore spaces and the configuration between spherical pores and cylinder pores is good, corresponds to the most possible pore structure, hence, relative ideal seepage characteristics; on the third pathway (on the bottom), cylinder pores are developed within small pores and spherical pores are dominated within big pores, corresponds to bad seepage characteristics.
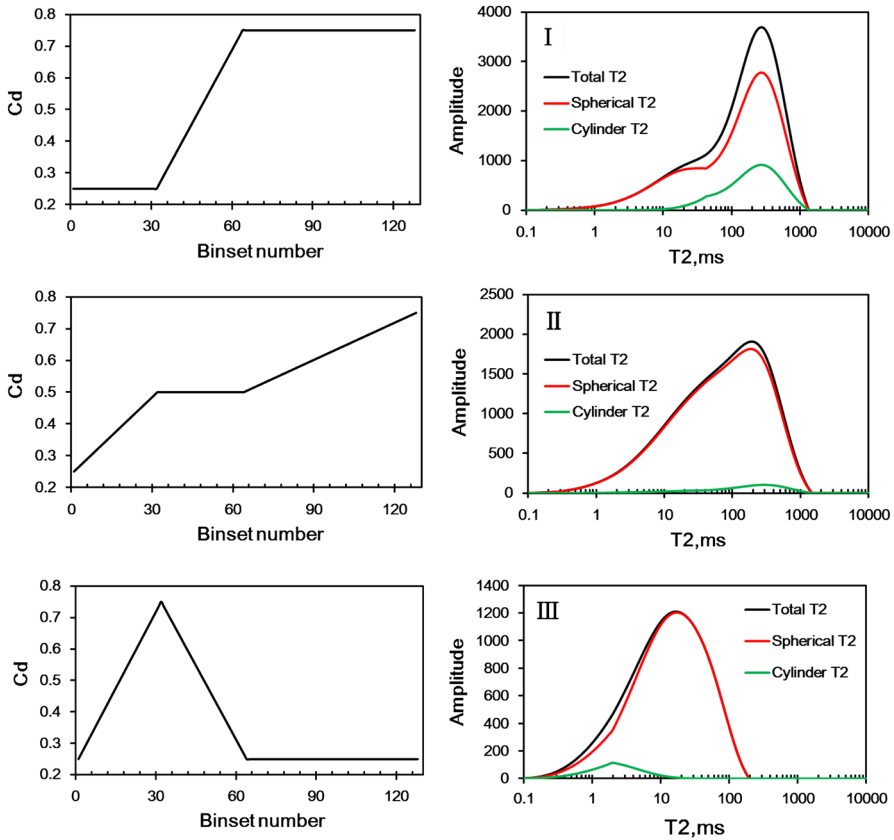
Fig. 4 Different pathway corresponds to different pore structure

In order to understand the pore structure more clearly, MICP (Mercury Injection Capillary Pressure) curve is used with the pressure from 0.01 to 32.1 MPa, as is shown in Fig. 5. From the figure, we know that plug I is dominated by meso and macro pores; plug II is dominated by meso and micro pores; plug III is dominated by micro pores. This illustrates the rationality of seepage characteristics analysis above.

4 Core Plugs Analysis and Field Data Processing

Utilizing the method mentioned previously, the detailed analysis of pore structure is performed for the 8 core plugs, including the three plugs above. The permeability and porosity of the 8 core samples are presented in Table 1. Here, Φ_C is the cylinder porosity, which is calculated by the sum of cylinder T_2 spectrum amplitude values multiplied by corresponding calibration factor.
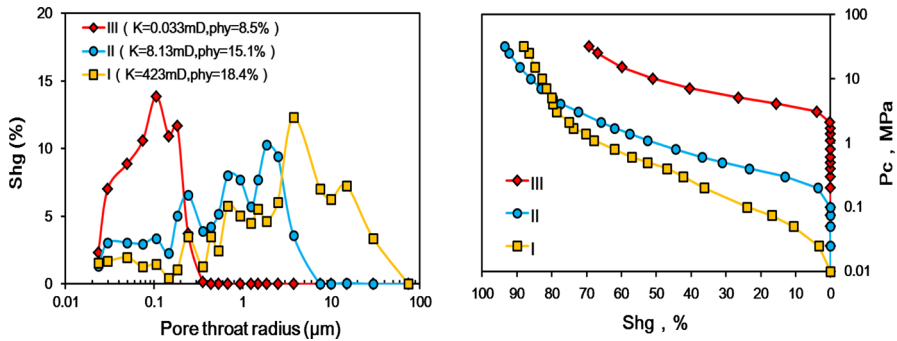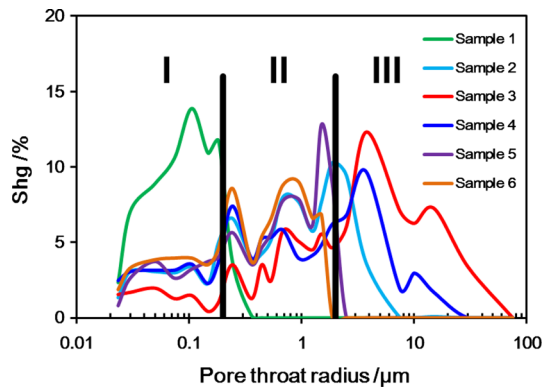
Fig. 5 Pore throat distribution (*left*) and MICP curve (*right*)

Table 1 Permeability and porosity of the 8 core plugs

Sample	1	2	3	4	5	6	7	8
k (10^{-3} μm^2)	0.033	8.13	423	6.39	10.2	3.28	6.51	333
Φ, %	8.48	15.06	18.4	13.2	13.6	12.8	14.1	17.7
Φ_C, %	0.95	1.69	9.51	0.59	1.53	0.56	0.80	9.21

Fig. 6 Pore throat distribution curve of 6 core samples

Mercury injection data have been obtained for only six core samples (Fig. 6), and the pore throat distribution curves of the six core samples can be divided into three types. Type I corresponds to micro pore throat only (sample 1), Type II corresponds to micro and meso pore throat with little macro pore throat (sample 2, sample 5 and sample 6), and Type III corresponds to the whole size pore throat while the main peaks are in macro pore throat (sample 3 and sample 4).

By combining pore throat distribution curves and porosities, several qualitative judgments can be concluded. Type I corresponds to poor permeability regardless of whether cylinder pore exists. Type II corresponds to some certain permeability if cylinder pore is developed in meso pores; otherwise, the same situation as type 1

applies. Finally, Type III corresponds to fairly good permeability if cylinder pore is developed in meso and macro pores; otherwise, the permeability will be ordinary.

In Fig. 7, T_2 decomposition spectrums of the eight core samples are presented. Obviously, it can be seen that (a) sample 1 corresponds to a short relaxation time to the left ($T_2 < 200$ ms). Micro cylinder pores are abundantly developed in micro pores ($T_2 < 10$ ms), and sphere pore is developed in meso pores ($T_2 > 10$ ms) with few cylinders. It can be concluded that the pore connectivity is poor, and the permeability is also low. The result is consistent with that of core experimental analysis. Sample 2 and sample 5 correspond to the wide T_2 distribution with a relaxation time ranging from 0.2 to 2000 ms. The cylinder pore is partly developed in meso and macro pores ($T_2 > 10$ ms), and the cylinder pore is dominant in micro pores ($T_2 < 10$ ms) with small cylinder pores. It can be concluded that both the pore connectivity and permeability are mediocre. The result is consistent with that of core experimental analysis. Sample 4 and sample 6 correspond to the total T_2 distribution ranges from 1 to 900 ms. The cylinder pores are partly developed in meso and macro pores. It can be concluded that the pore connectivity is mediocre and permeability is also mediocre. Combining the cylinder porosity in Table 1, we can determine that the permeability of sample 4 and sample 6 is slightly lower than that of sample 2 and sample 5. The result is in accordance with that of core experimental analysis. Sample 3 and sample 8 correspond to the whole T_2 spectrum ranging from 1 to 2000 ms. Cylinder and sphere pores are abundantly developed in meso and macro pores ($T_2 \geq 10$ ms). It can be drawn out that the pore connectivity seems to be better in addition to permeability. The result is consistent with that of core experimental analysis. Finally, sample 7 is considered. The whole T_2 spectrum ranges from 0.2 to 600 ms, and only in micro pores are the cylinder pores developed, which is similar to sample 1. Combining the porosity value in Table 1, the permeability of sample 7 should be larger than that of sample 1, which is supported by core experimental analysis.

Based on the comprehensive analysis above, we can directly estimate the connectivity and permeability of the formation to determine the 'sweet spot' in logging interpretation via the NMR T_2 spectrum decomposition technology. The specific judgment standard is the cylinder pores are abundantly developed in meso and macro pores. What can be seen in T_2 distribution is that the cylinder T_2 spectrum is located to the right with high T_2 relaxation time and high peak values.

We make the corresponding program with computer language and realize the field NMR logging data progressing on the CIFLog software platform (Fig. 8). From this figure, the cylinder T_2 spectrum distribution of interval I locates to the right side of the track, which means that the cylinder pore is developed in meso and macro pores, which is an indication of a good connectivity and permeability. In the interval II, the total T_2 distribution is wide and some cylinder pore is developed in micro pores, as well as in meso and macro pores. Compared with interval I, interval II does not have the same good connectivity and permeability. Therefore, interval I is the 'sweet spot' of the formation, which is in accordance with the conventional interpretation of permeability.
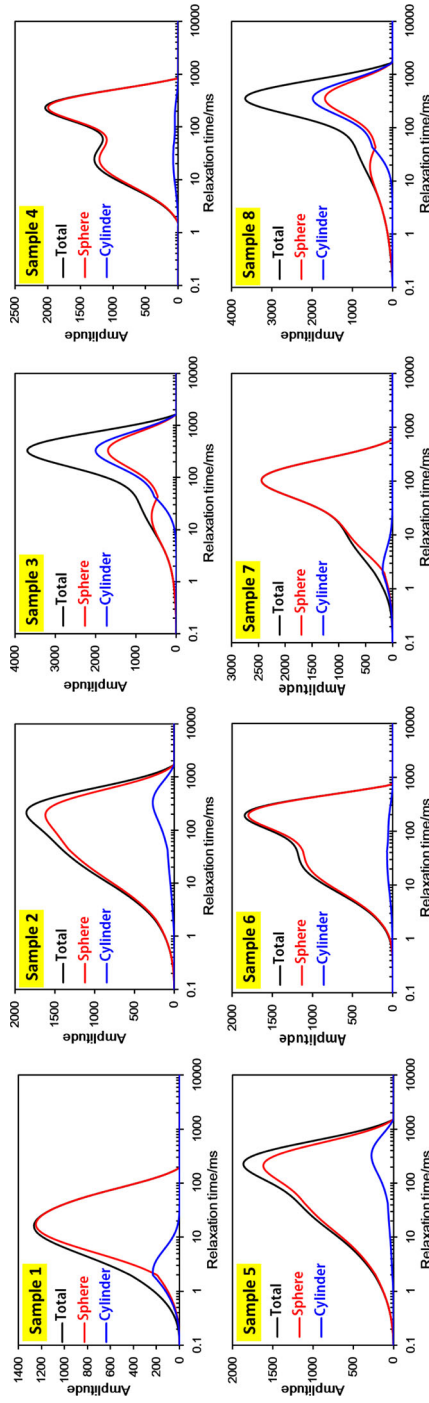
Fig. 7 Total T_2 spectrum and decomposed sphere and cylinder T_2 spectrum
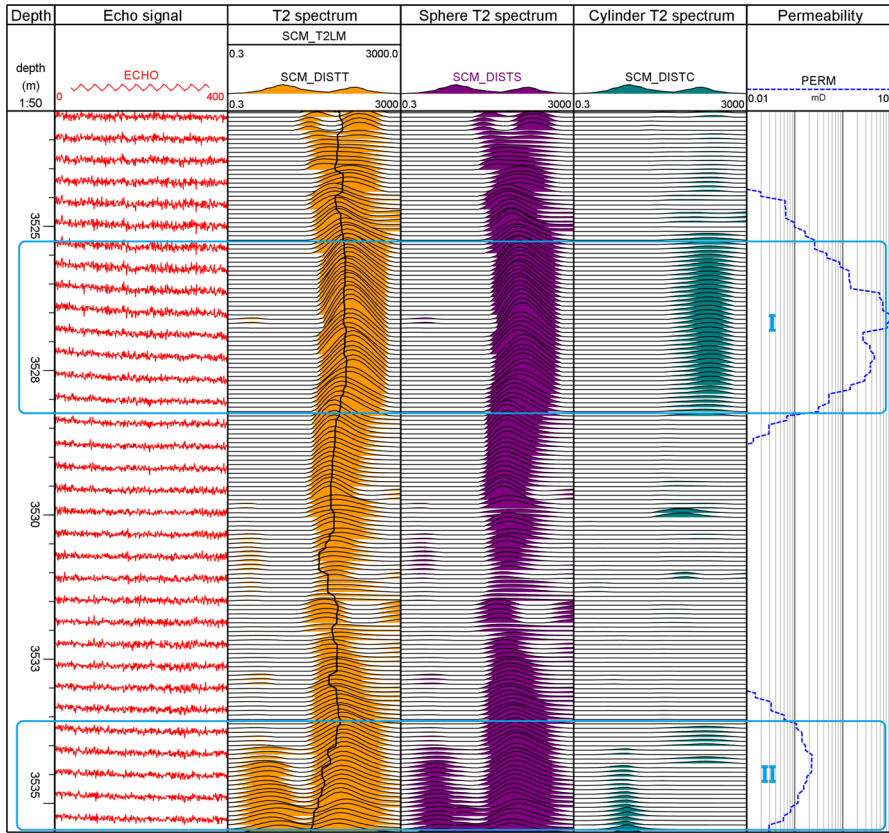
Fig. 8 Field NMR logging data processing with NMR pore structure program

5 Conclusions and Discussion

The capillary bundle model is oversimplified, but it is easily solved in mathematics and is acceptable to geologists. The pore network model is more exact than the capillary bundle model in the description of formation pore structure. However, this model is limited to simulation study, and it is also difficult to apply in field logging data interpretation. The Sphere–Cylinder model is an optimization of the two models and has been capable of processing field NMR logging data.

In this paper, we design the pathway of C_d route in the Sphere–Cylinder model and analyze different pathway corresponds to different pore structure. Specifically, pore structure and seepage characteristics of 8 core plugs are analyzed, and the estimation conclusions is quite in accordance with that of core experimental analysis, including NMR experiment and MICP curves. Consequently, the pore connectivity and permeability can be directly evaluated by the decomposed cylinder T_2 spectrum distribution. The 'sweet spot' may be recognized when cylinder T_2 spectrum locates to the right side of a track with high T_2 relaxation time and peak

values. The technology proposed in this paper provides a new algorithm and theoretical basis in the direct estimation of pore structure via NMR logging data. Nevertheless, it is only a qualitative conclusion. To be quantitative, more research is still required, e.g. whether the constraint condition is reasonable or not.

Appendix 1

The conjugate gradient (CG) method is proposed by Hesteness and Stiefel for solving linear system of equations [27]. Here, we use this method to inverse the relaxation signal to obtain T_2 distribution.

As mentioned previously, the observed relaxation signal is modeled as multi-exponential decay:

$$
\begin{aligned}
\text{echo}_1 &= \varphi_1 e^{-t_1/T_{2,1}} + \varphi_2 e^{-t_1/T_{2,2}} + \cdots + \varphi_n e^{-t_1/T_{2,n}} \\
\text{echo}_2 &= \varphi_1 e^{-t_2/T_{2,1}} + \varphi_2 e^{-t_2/T_{2,2}} + \cdots + \varphi_n e^{-t_2/T_{2,n}} \\
&\cdots \qquad\qquad \cdots \qquad\qquad \cdots \\
\text{echo}_m &= \varphi_1 e^{-t_m/T_{2,1}} + \varphi_2 e^{-t_m/T_{2,2}} + \cdots + \varphi_n e^{-t_m/T_{2,n}}
\end{aligned}
\tag{12}
$$

where m and n are echo number and T_2 bin set number, respectively; t_i ($i = 1,2,...,m$) is the measured time of i-th echo, which is the integer multiple of inter-echo spacing time T_E; T_{2j} ($j = 1,2,...,n$) is the bin set value with equal space after taking logarithm.

Equation (12) can be rewritten as:

$$
\begin{aligned}
&b_{m\times 1} = A_{m\times n} x_{n\times 1} \\
&\lg(T_{2j}) = \lg(T_{2\min}) + \frac{j-1}{n-1}(\lg(T_{2\max}) - \lg(T_{2\min})) \\
&b_{m\times 1} = (\text{echo}_1, \text{echo}_2, \ldots, \text{echo}_m)^T, \quad x_{n\times 1} = (\varphi_1, \varphi_2, \ldots, \varphi_n)^T \\
&A_{m\times n} = \begin{bmatrix} e^{-t_1/T_{21}} & e^{-t_1/T_{22}} & \cdots & e^{-t_1/T_{2n}} \\ e^{-t_2/T_{21}} & e^{-t_2/T_{22}} & \cdots & e^{-t_2/T_{2n}} \\ \vdots & \vdots & \ddots & \vdots \\ e^{-t_m/T_{21}} & e^{-t_m/T_{22}} & \cdots & e^{-t_m/T_{2n}} \end{bmatrix}
\end{aligned}
\tag{13}
$$

The algorithm flow of conjugate gradient method can be summarized as:

1. Initializing: $x_0 \in R^n$, $r_0 = b - Ax_0$, $d_0 = A^T r_0$, the maximum iterations k_{max}, the error constant err; $k = 0$, begin the iteration;
2. If $\|r_k\| < err$, terminate the iteration and output x_k; otherwise, go on;
3. $\alpha_k = A^T r_{k-1}^2 / A d_{k-1}^2$, $x_k = x_{k-1} + \alpha_k d_{k-1}$, $r_k = r_{k-1} - \alpha_k A d_{k-1}$;
4. $\beta_k = \|A^T r_k\|^2 / \|A r_{k-1}\|^2$, $d_k = A^T r_k + \beta_k d_{k-1}$;
5. $k = k+1$; go back to 2).

References

1. Z.T. Luo, R.C. Wang, *Pore Structure of Oil and Gas Reservoir* (Beijing Science Press, Beijing, 1986)
2. K. Verwer, G.P. Eberli, R.J. Weger, AAPG Bull. **95**(2), 175–190 (2011)
3. H.L. Bian, J. Guan, Z.Q. Mao, X.D. Ju, G.Q. Han, Appl. Geophys. **11**(4), 374–383 (2014)
4. A. Sakhaee-Pour, S.L. Bryant, AAPG Bull. **98**(4), 663–694 (2014)
5. T.Y. Liu, T.Z. Tang, H.H. Du, H.N. Zhang, H.T. Wang, Chin. J. Geophys. (in Chinese) **56**(5), 674–684 (2013)
6. Z.Q. Mao, L. Xiao, Z.N. Wang, J. Yan, X.G. Liu, B. Xie, Appl. Magn. Reson. **44**(4), 449–468 (2012)
7. C.L. Li, C.C. Zhou, L. Xia, F.L. Hu, L. Zhang, W.J. Wang, Appl. Geophys. **7**(3), 283–291 (2010)
8. R. Rezaee, A. Saeedi, B. Clennell, J. Pet. Sci. Eng. **88–89**(2), 92–99 (2012)
9. A. Valori, F. Ali, A. Al-Zoukani, R. Taherian, NMR Measurements for Pore Size Mapping at Fine Scale, in IPTC 2014: International Petroleum Technology Conference, Session 26: RESERVOIR - Geological Modelling: Formation Evaluation (EAGE, 2014)
10. C. Lu, Z. Heidari, Quantifying the Impact of Natural Fractures and Pore Structure on NMR Measurements in Multiple-Porosity Systems, in IPTC 2014: International Petroleum Technology Conference, Session 23: E&P Geoscience - Tectonic History and Basin Evolution (EAGE, 2014)
11. G.R. Coates, L.Z. Xiao, M.G. Prammer, *NMR Logging Principles and Applications* (Gulf Publishing Company, Texas, 1999)
12. K.R. Brownstein, C.E. Tarr, Phys. Rev. A **19**(6), 2446–2453 (1979)
13. W.F.J Slijkerman, J.P Hofman, W.J Looyestijn, Y. Volokitin, Petrophysics **42**(4):334–343 (2001)
14. T.Y. Liu, S.M. Wang, R.S. Fu, Oil Geophys. Prospect. **38**(3), 328–333 (2003)
15. Y.D. He, Z.Q. Mao, L.Z. Xiao, X.J. Ren, Chin. J. Geophys. (in Chinese) **48**(2), 412–418 (2005)
16. R.L. Kleinberg, W.E. Kenyon, P.P. Mitra, J. Magn. Reson. **108**(2), 206–214 (1994)
17. R.L. Kleinberg, M.A. Horsfield, J. Magn. Reson. **1990**(88), 9–19 (1969)
18. K.J. Dunn, D.J. Bergman, G.A. Latorraca, *Nuclear Magnetic Resonance: Petrophysical and Logging Applications* (Elsevier Science, Pergamon, 2002)
19. B. Kenyon, R. Kleinberg, C. Straley, G. Gubelin, C. Morriss, Oilfield Rev. **7**(3), 19–33 (1995)
20. E. Grunewald, R. Knight, Geophysics **74**(6), E215 (2009)
21. I. Fatt, The Network Model of Porous Media. I, II & Iii, Petrol Trans Aime. **207**:144–177 (1956)
22. W. Kewen, L. Ning, Appl. Geophys. **5**(2), 86–91 (2008)
23. T.Y. Liu, L.Z. Xiao, R.S. Fu, Z.D. Wang, Chin. J. Geophys. (in Chinese) **47**(4), 663–671 (2004)
24. C.C. Zhou, T.Y. Liu, Acta Pet. Sin. **27**(1), 92 (2006)
25. T.Y. Liu, C.C. Zhou, Z.T. Ma, G.Q Liu, J. Tongji Univ. (Nat. Sci. Ed.) **34**(11), 1464–1469 (2007)
26. X. Ge, Y. Fan, Y. Cao, Y. Xu, X. Liu, Y. Chen, Appl. Magn. Reson. **2**, 155–167 (2014)
27. M.R. Hestenes, E. Stiefel, J. Res. Natl. Bur. Stand. **49**(6), 99–147 (1952)